Monthly Notices
of the
ROYAL ASTRONOMICAL SOCIETY

MNRAS **490,** L12–L16 (2019) doi:10.1093/mnrasl/slz140

Super-giant pulses from the Crab pulsar: energy distribution and occurrence rate

Apurba Bera ★ and Jayaram N. Chengalur

National Centre for Radio Astrophysics, Tata Institute of Fundamental Research, Ganeshkhind, Pune 411007, India

Accepted 2019 August 28. in original form 2019 August 17

ABSTRACT

We present statistical analysis of a fluence-limited sample of over 1100 giant pulses from the Crab pulsar, with fluence $>$ 130 Jy ms at $\sim$1330 MHz. These were detected in $\sim$260 h of observation with the National Centre for Radio Astrophysics (NCRA) 15 m radio telescope. We find that the pulse-energy distribution follows a power law with index $\alpha \approx -3$ at least up to a fluence of $\sim$5 Jy s. The power-law index agrees well with that found for lower-energy pulses in the range 3–30 Jy ms. The fluence distribution of the Crab pulsar hence appears to follow a single power law over $\sim$3 orders of magnitude in fluence. We do not see any evidence for the flattening at high fluences reported by earlier studies. We also find that, at these fluence levels, the rate of giant-pulse emission varies by as much as a factor of $\sim$5 on time-scales of a few days, although the power-law index of the pulse-energy distribution remains unchanged. The slope of the fluence distribution for Crab giant pulses is similar to that recently determined for the repeating FRB 121102. We also find an anti-correlation between the pulse fluence and the pulse width, so that more energetic pulses are preferentially shorter.

Key words: pulsars: general – pulsars: individual (Crab) – radio continuum: transients.

1 INTRODUCTION

The Crab pulsar is one of a handful of pulsars known to emit giant radio pulses (e.g. Ershov & Kuzmin 2005; Kazantsev & Potapov 2017; Mahajan et al. 2018; McKee et al. 2019). The giant pulses of the Crab pulsar reach flux densities several orders of magnitude higher than the average pulses (e.g. Hankins et al. 2003; Jessner et al. 2005; Hankins & Eilek 2007; Crossley et al. 2010). Crab giant pulses are known to occur during both the pulsar's main pulse and the inter-pulse emission window, although compared to the main pulse, the frequency of occurrence is about an order of magnitude lower in the inter-pulse window (Karuppusamy, Stappers & van Straten 2010). The relatively high rate of giant-pulse emission makes the Crab pulsar best suited for statistical studies on giant pulses. In earlier studies, giant pulses have been found to show different statistical properties from those shown by regular pulses. For example, the pulse-energy distribution of giant pulses follows a power law (e.g. Popov & Stappers 2007; Bhat, Tingay & Knight 2008; Karuppusamy et al. 2010), while that of regular pulses follows exponential or lognormal distributions (e.g. Hesse & Wielebinski 1974; Ritchings 1976), This indicates that normal and giant pulses probably arise from different emission mechanisms.

In this letter, we present a statistical study of super-giant pulses (SGPs, fluence $\gtrsim$ 100 Jy ms) from the Crab pulsar detected at $\sim$ 1.4 GHz in $\sim$ 260 h of observation, with pulse energies up to two orders of magnitude above the energy range explored in similar studies in the literature. We compare the statistical properties of the super-giant pulses that we detect against those of their weaker cousins as well as the currently known properties of fast radio bursts, for which one proposed model is super-giant pulses from young pulsars or magnetars (e.g. Lyutikov, Burzawa & Popov 2016).

2 OBSERVATIONS AND DATA PROCESSING

The Crab pulsar was observed for $\approx$ 260 h in 31 observing sessions of typically 6–9 h duration. The observations spanned $\approx$ 45 d in 2019 February–April and were carried out with the National Centre for Radio Astrophysics (NCRA) 15 m telescope located in the NCRA campus in Pune, India. The observing bandwidth was 100 MHz between 1280 and 1380 MHz, (of which $\sim$65 MHz is usable). Throughout the observing period, the telescope sensitivity (i.e. $G/T_{\rm sys}$) was measured using known bright radio sources – Cygnus-A, Cassiopeia-A and the Crab nebula. The sensitivity at 1330 MHz was measured to be $G/T_{\rm sys} \approx 3.4 \times 10^{-4}\ Jy^{-1}$ and was also constant to within 10 per cent over this period.

2.1 Real-time and offline processing

Real-time processing of the data was done using REDSPIDER-15m (REal-time De-disperser and Single Pulse IDentifiER) software developed by us for the NCRA 15 m telescope. The software

★ E-mail: apurba@ncra.tifr.res.in (AB); chengalur@ncra.tifr.res.in (JNC)

takes the Nyquist-sampled data and computes the co- and cross-polar 128 channel spectra, which are averaged to a time resolution of ≈80 μs. After RFI rejection to exclude narrow-band as well as bursty broad-band RFI, the data are incoherently de-dispersed. For our observing set-up the intra-channel dispersion ($\sim$ 160 μs) is much larger than the intrinsic width of the Crab giant pulse (i.e. $\sim$ few μs). The incoherent de-dispersion was done at a fixed dispersion measure (DM) (i.e. that corresponding to the DM of the Crab pulsar, i.e. 56.77 pc cm^{-3}; e.g. Bilous et al. 2016). The two circular polarizations are averaged to produce the Stokes I time series, which is searched for giant-pulse candidates, which are required to (1) have S/N > 8, and (2) be brighter at the true DM than at DMs 5 pc cm^{-3} above and below the true DM. An identical search is carried out on the time series after smoothing it by a boxcar kernel of width 2, with the same threshold for minimum S/N. (Recall that the observed pulse width is dominated by intra-channel dispersion, which is $\sim$2 times the time resolution.) The typical RMS noise of the system for a time resolution of ≈ 80 μs is ≈ 54 Jy. The detection threshold (S/N > 8) corresponds to a limiting fluence of ≈ 100 Jy ms for a time resolution of ≈ 160 μs (after smoothing the time series). As the observed pulse width is dominated by intra-channel dispersion smearing, our detection threshold corresponds to a fluence and not a flux threshold. For all candidate giant pulses, ≈ 150 ms (i.e. ≈ three times as long as the dispersion sweep time across the observation band for the DM of Crab) of Nyquist-sampled raw data, centred at the pulse arrival time, is written to the disk for offline processing. All subsequent analysis uses the offline processed data. The data for each candidate pulse are coherently de-dispersed (yielding a time resolution of $\sim$80 ns) and then visually examined to reject spurious pulses. About 20 per cent of the candidate pulses detected in the real-time pipeline are found to be spurious, most of which are close to the detection threshold.

3 RESULTS AND DISCUSSION

3.1 Pulse shapes

Our final sample consists of 1799 giant pulses from the Crab pulsar detected in our observation. We have not aligned these pulses with respect to the average Crab pulse, and hence the pulses that we detect correspond to giant pulses from both the main pulse and the inter-pulse. However, as noted above, earlier studies have shown that only $\sim$10 per cent of the pulses correspond to the inter-pulse window. Our S/N threshold of 8 (at a time resolution of 160 μs) corresponds to a fluence threshold of $\gtrsim$ 100 Jy ms. However, for all of the following analysis, we conservatively include only pulses with fluence $\geq$ 130 Jy ms (corresponding to S/N $\gtrsim$ 10) in order to avoid incompleteness effects near the detection threshold. This yielded a complete sample of 1153 giant pulses with fluence $\geq$ 130 Jy ms.

Four example pulses are shown in Fig. 1. The detected pulses show a wide variety of temporal structures including single-component pulses and multi-component pulses with a strong burst preceded or followed by one or more weaker components. Each component shows narrow spiky features at much smaller time-scales. The pulse seen in Fig. 1(a) shows a sharp rise followed by a slower decline, consistent with what would be expected from scattering. This is typical for all the single-component pulses that we see. The pulse profiles that we see are broadly similar to those observed by Sallmen et al. (1999). These authors discuss possible origins for the multiple components as well as the exponential-like decay, concluding that the decay probably arises from scattering while the multiple components are likely intrinsic (and not copies caused by refraction/diffraction in discrete regions of enhanced density).

3.2 Pulse-energy distribution

We measure the fluence (which we use interchangeably with 'pulse energy') by integrating all the flux within a time interval of $\sim$3 ms (i.e. ≈ the width of the average pulse profile) centred on each detected pulse. The maximum separation of components in the multi-component pulses is $\sim$30 μs, well within our integration interval. The most energetic pulse in our sample has a fluence ≈ 4.7 Jy s and a peak flux density of ≈4 MJy. This is among the brightest known giant pulses of the Crab pulsar detected at $\sim$1.4 GHz. We parametrize the pulse-energy distribution as

$$N(E)\mathrm{d}E \propto E^{\alpha}\mathrm{d}E \quad (1)$$

where E is the fluence and $N(E)$ is the number of pulses per unit time per unit fluence. The fluence distribution, along with the best-fitting power law, which has a slope of $\alpha = -2.81 \pm 0.05$, is shown in Fig. 2. The slope that we find is within the range of that observed earlier for giant pulses with much lower fluences (e.g. Popov & Stappers 2007; Bhat et al. 2008; Karuppusamy et al. 2010; Mickaliger et al. 2012; Rudnitskii, Popov & Soglasnov 2017). Cordes et al. (2004) and Mickaliger et al. (2012) had seen signatures of flattening of the slope at high pulse energies, and had dubbed the giant pulses with fluxes above this flattening as 'super-giant pulses'. Both papers measure the pulse energies in terms of S/N ratios, which makes a direct comparison with our measurement difficult. However, the NCRA 15 m with a 65 MHz usable bandwidth is about a factor of $\sim$8 less sensitive than the system used by Mickaliger et al. (2012) (i.e. the NRAO 140 ft with a 400 MHz usable bandwidth) even after accounting for the contribution of the Crab nebula to the system temperature (see e.g. the discussion in Cordes et al. 2004). Mickaliger et al. (2012) see a flattening of the energy distribution at a S/N of $\sim$80 (see their fig. 6), which corresponds to about S/N ≈10 for us, i.e. at fluences below what we are analysing here. Our large sample of bright pulses does not show any signature of this flattening.

3.3 Pulse fluence and width

In situations where the pulse width is set entirely by scattering, one would expect that the pulse width would be independent of the fluence. We define the 'effective width' (w_e) as the ratio of the fluence and peak flux density. Fig. 3 shows a scatter plot of effective width and fluence. As can be seen, we see a clear anti-correlation, indicating that brighter pulses tend to be narrower. The widths that we use average over the multiple components of the profile. Sallmen et al. (1999) used a parametric model to decompose complex profiles into multiple components. From the best-fit parameters to each component they found that the widths did not correlate with the fluence, and argued that this supported the conclusion that the pulse widths were dominated by scattering. We defer modelling of the profiles to a later paper, but our result here shows that over the pulse as a whole, the fluence anti-correlates with the width. Popov & Stappers (2007) found a similar result for weaker giant pulses from the Crab pulsar. Given the large number of pulses that we detect, we can also look at the relationship between width and fluence in some detail. We show in Fig. 4 the fluence distribution for different pulse widths. As can be seen, the pulse-energy distribution is steeper for larger pulse widths, consistent with the anti-correlation between

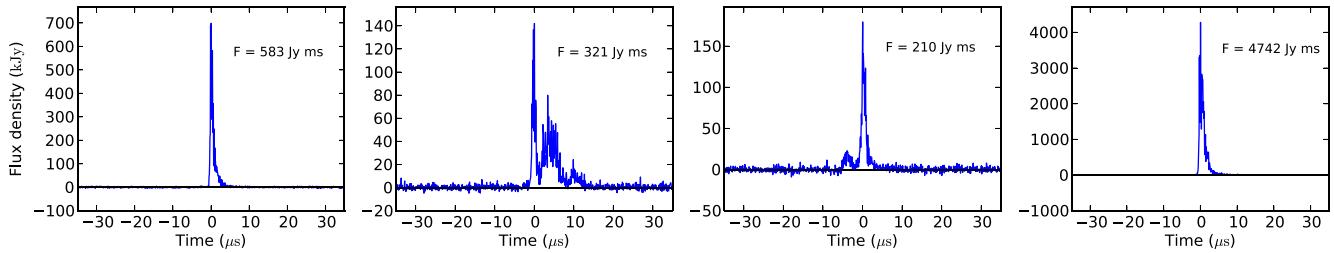

Figure 1. Examples of super-giant pulses detected in our observation. From left to right – [1] a typical single-component pulse showing clear evidence of a scattering tail, [2] a multi-component pulse with weaker trailing components, [3] a multi-component pulse with a weaker leading component and [4] the most energetic super-giant pulse detected in the observation. The last one is also one of the most energetic giant pulses observed from the Crab pulsar at frequencies ∼1.4 GHz.

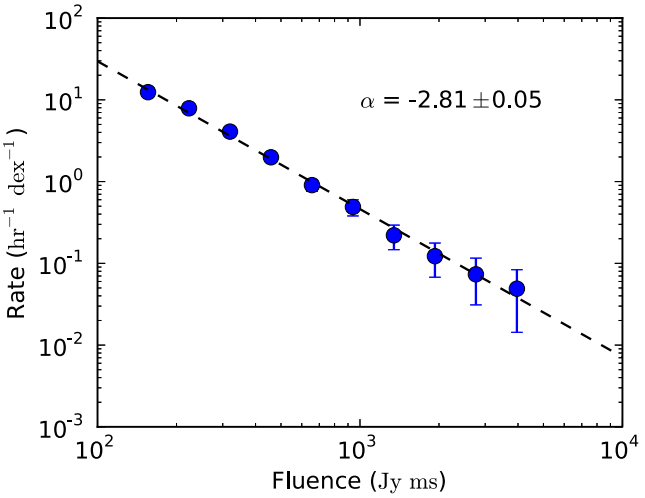

Figure 2. Fluence distribution of the super-giant pulses from the Crab pulsar for fluence $F > 130$ Jy ms. The uncertainties associated with the data points correspond to Poisson errors. The dashed line shows a power-law fit to the distribution with best-fitting power-law exponent $\alpha \approx -2.8$.

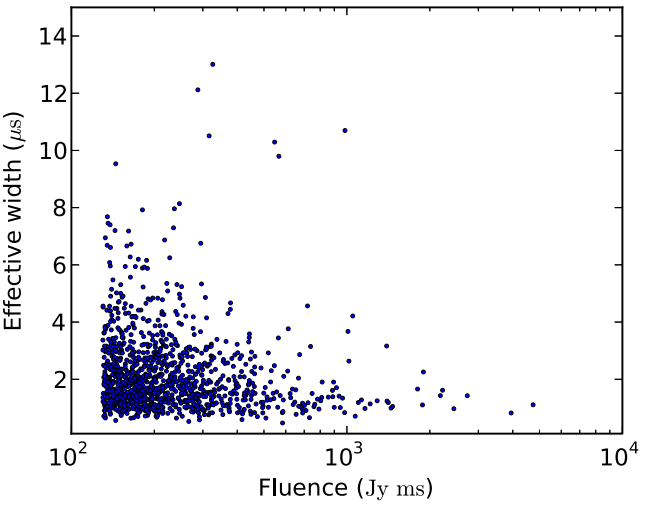

Figure 3. Scatter plot of effective width (fluence/peak) and fluence of 1153 super-giant pulses with fluence >130 Jy ms. The effective width ranges from $\lesssim$1 μs to ∼ 10 μs, but most of the pulses have widths between 1 and 2 μs.

pulse width and fluence. This anti-correlation is in contrast with the situation for FRB pulses, where recent studies indicate that the pulse width appears to weakly correlate with the pulse luminosity (Hashimoto et al. 2019). Finally, we note that Fig. 3 shows that the typical effective width of our giant pulses is between 1–2 μs, although there are pulses narrower than 1 μs and as wide as ≈10 μs. This is within the range of scatter broadening of the Crab giant pulses reported by Rudnitskii et al. (2017).

3.4 Occurrence rate

The giant-pulse occurrence rate varies between the different observing sessions. Fig. 5 shows the average rate of occurrence of pulses (with fluence > 130 Jy ms) in each observing session (of ∼6–9 h duration) as a function of the mean MJD of the observing sessions. The average occurrence rate appears to vary on a time-scale of a few days, by as much as a factor of ∼ 5. Kazantsev, Potapov & Pshirkov (2019) also find a similar irregular variation in the rate of Crab giant pulses. In Fig. 6 we show the pulse-energy distribution separately for days when the occurrence rate was high (58521 < MJD < 58526) and when the occurrence rate was low (58579 < MJD < 58589). We find that although the occurrence rate has changed, the power-law index is constant within the uncertainties. This suggests that while the efficiency of the giant-pulse emitting process appears to vary on a time-scale of a few days, the intrinsic properties of the underlying process itself do not change. The intrinsic properties of the process may, however, evolve over longer time-scales; Rudnitskii et al. (2017) show variations in the slope of the pulse-energy distribution for observations spread over a few years (albeit for pulses significantly weaker than those analysed here).

3.5 Crab giant pulses and FRBs

The brightest pulse detected in our observation has a fluence of ≈ 4.7 Jy s. Modern FRB surveys have fluence limits of typically ≈ few Jy ms (e.g. Keane & Petroff (2015)). A pulse of fluence similar to the brightest pulse that we have observed could only be detected to a distance of a few tens of kpc in these surveys. Models of FRBs that involve giant pulses from compact magnetized objects hence typically require sources with much higher magnetic fields, such as magnetars or extremely young pulsars (Connor, Sievers & Pen 2016; Cordes & Wasserman 2016; Katz 2016; Lyutikov et al. 2016). In this context, it is interesting that the the pulse-energy distribution of the repeating FRB121102 (Spitler et al. 2014, 2016), is well described by a power law with index $\alpha = -2.8 \pm 0.3$ (Gourdji et al. 2019), in excellent agreement with what we find for the Crab

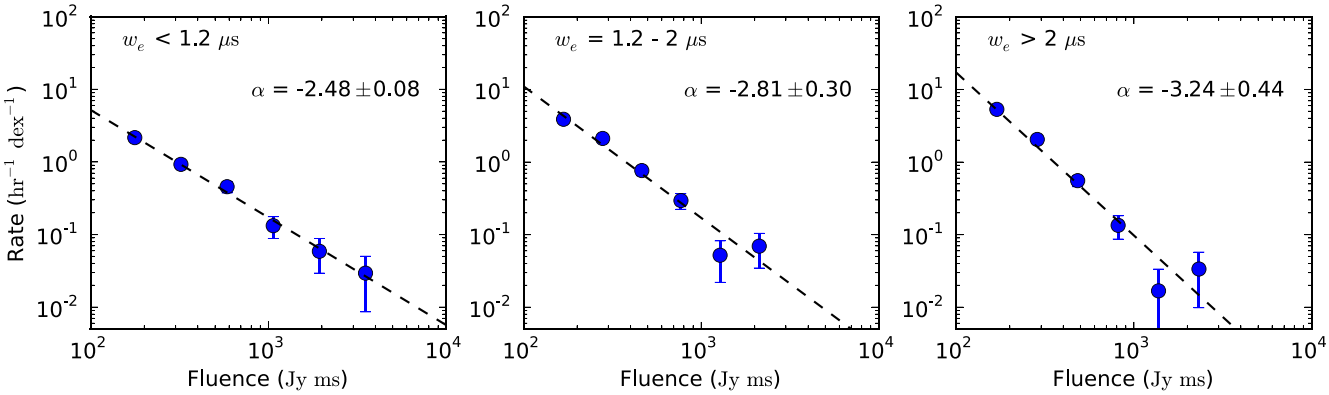

Figure 4. Fluence distribution of the super-giant pulses (fluence $F > 130$ Jy ms) for different effective widths, <1.2 μs, 1.2–2 μs and >2 μs, respectively. The best-fitting power-law index for each case is mentioned in the corresponding panel. The power-law index is steeper for larger effective widths, which implies that more energetic pulses are predominantly shorter. This trend is also apparent in Fig. 3.

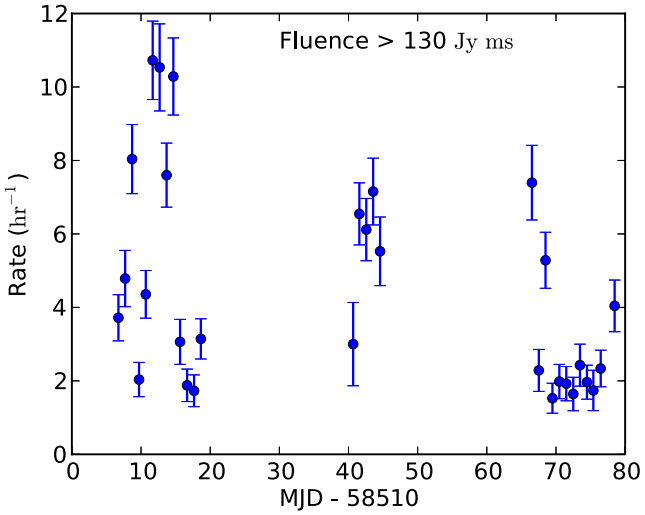

Figure 5. Average rate of super-giant pulses (with fluence > 130 Jy ms) from the Crab pulsar in different observing sessions during 2019 February–April as a function of the mean MJD of the observing sessions. Each observing session is typically 6–9 h long. The uncertainties associated with data points correspond to Poisson errors. The blank days show when no observation was done.

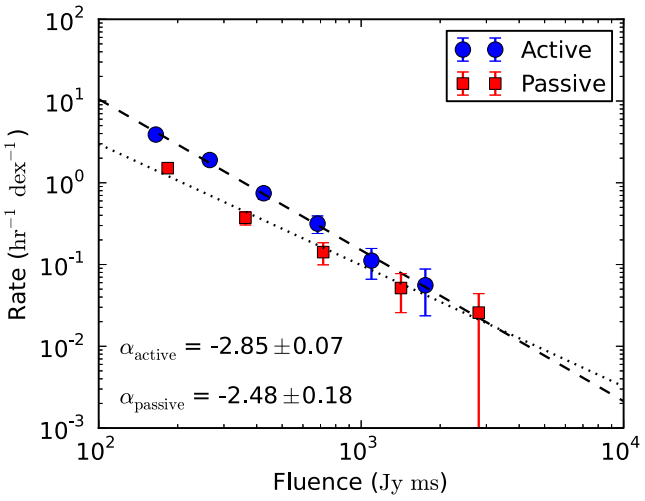

Figure 6. Fluence distribution of the super-giant pulses (above fluence $F >$ 130 Jy ms) between 58521 < MJD < 58526 ('active' phase) and between 58579 < MJD < 58590 ('passive' phase). The uncertainties associated with the data points correspond to Poisson errors. The dashed lines show power-law fits to the distributions. The best-fitting power-law exponent remains the same within the uncertainties in both the phases.

giant pulses. Further, like the Crab giant pulses, the burst rate from FRB121102 also appears to vary with time (Scholz et al. 2016; Oppermann, Yu & Pen 2018). Although only a small fraction of the currently known FRBs have been known to repeat, the possibility that all FRBs repeat cannot be ruled out with currently available data (e.g. Caleb et al. 2019). However, the non-detection of repeating bursts in long follow-up observations of some of the known non-repeating FRBs, with instruments sensitive enough to detect much fainter bursts than the original event, have put strong constraints on their repetition rates (e.g. Petroff et al. 2015). Reconciling these observations with giant-pulse-like sources would be easier if the pulse-energy distribution were to flatten at high fluences. In 260 h of observation of the Crab pulsar we see no evidence for any such flattening even at fluences as high as ∼ 5 Jy s. However, if the repeating FRBs belong to a different class to the non-repeating ones, our results suggest that super-giant pulses emitted from highly energetic young pulsars or magnetars continue to be a viable model for repeating FRBs.

4 CONCLUSIONS

We have studied the pulse energy and occurrence rate statistics on a sample of 1153 giant pulses of the Crab pulsar, complete down to fluence > 130 Jy ms, detected in ∼ 260 h of observation at ∼ 1330 MHz with the NCRA 15 m telescope. From these and earlier published results we find that the pulse-energy distribution of the giant pulses follows a power law with index $\alpha \sim -3$ from pulse energies of ∼ 3 Jy ms all the way up to ∼ 5 Jy s, spanning three orders of magnitude in fluence. We find no evidence for the earlier reported flattening of the distribution at high fluences. The power-law index is steeper for wider pulses, implying that more energetic pulses are preferentially narrower. We also observe that the average giant-pulse occurrence rate varies by as much as a factor of ∼ 5 on a time-scale of a few days, although the power-law index of the pulse-energy distribution does not vary. This power-law index is in good agreement with that recently determined for the repeating FRB 121102.

ACKNOWLEDGEMENTS

We thank the staff members who have made these observations possible. The NCRA 15 m telescope is run by the National Centre for Radio Astrophysics of the Tata Institute of Fundamental Research. AB thanks Avishek Basu for useful discussions.

REFERENCES

Bhat N. D. R., Tingay S. J., Knight H. S., 2008, ApJ, 676, 1200
Bilous A. V. et al., 2016, A&A, 591, A134
Caleb M., Stappers B. W., Rajwade K., Flynn C., 2019, MNRAS, 484, 5500
Connor L., Sievers J., Pen U.-L., 2016, MNRAS, 458, L19
Cordes J. M., Wasserman I., 2016, MNRAS, 457, 232
Cordes J. M., Bhat N. D. R., Hankins T. H., McLaughlin M. A., Kern J., 2004, ApJ, 612, 375
Crossley J. H., Eilek J. A., Hankins T. H., Kern J. S., 2010, ApJ, 722, 1908
Ershov A. A., Kuzmin A. D., 2005, A&A, 443, 593
Gourdji K., Michilli D., Spitler L. G., Hessels J. W. T., Seymour A., Cordes J. M., Chatterjee S., 2019, ApJ, 877, L19
Hankins T. H., Eilek J. A., 2007, ApJ, 670, 693
Hankins T. H., Kern J. S., Weatherall J. C., Eilek J. A., 2003, Nature, 422, 141
Hashimoto T., Goto T., Wang T.-W., Kim S. J., Wu Y.-H., Ho C.-C., 2019, MNRAS, 488, 1908
Hesse K. H., Wielebinski R., 1974, A&A, 31, 409
Jessner A., Słowikowska A., Klein B., Lesch H., Jaroschek C. H., Kanbach G., Hankins T. H., 2005, Advances Space Res., 35, 1166
Karuppusamy R., Stappers B. W., van Straten W., 2010, A&A, 515, A36
Katz J. I., 2016, Modern Phys. Lett. A, 31, 1630013
Kazantsev A. N., Potapov V. A., 2017, Astron. Rep., 61, 747
Kazantsev A. N., Potapov V. A., Pshirkov M. S., 2019, preprint (arXiv: 1905.05261)
Keane E. F., Petroff E., 2015, MNRAS, 447, 2852
Lyutikov M., Burzawa L., Popov S. B., 2016, MNRAS, 462, 941
Mahajan N., van Kerkwijk M. H., Main R., Pen U.-L., 2018, ApJ, 867, L2
McKee J. W. et al., 2019, MNRAS, 483, 4784
Mickaliger M. B. et al., 2012, ApJ, 760, 64
Oppermann N., Yu H.-R., Pen U.-L., 2018, MNRAS, 475, 5109
Petroff E. et al., 2015, MNRAS, 454, 457
Popov M. V., Stappers B., 2007, A&A, 470, 1003
Ritchings R. T., 1976, MNRAS, 176, 249
Rudnitskii A. G., Popov M. V., Soglasnov V. A., 2017, Astron. Rep., 61, 393
Sallmen S., Backer D. C., Hankins T. H., Moffett D., Lundgren S., 1999, ApJ, 517, 460
Scholz P. et al., 2016, ApJ, 833, 177
Spitler L. G. et al., 2014, ApJ, 790, 101
Spitler L. G. et al., 2016, Nature, 531, 202

This paper has been typeset from a TEX/LATEX file prepared by the author.